STUDIA UBB PHYSICA, Vol. 65 (LXV), 1-2, 2020, pp. 35-47
(RECOMMENDED CITATION)
doi:10.24193/subbphys.2020.05

ATTOSECOND INTERFEROMETRY USING A HHG-2ω_0 SCHEME*

V. LORIOT[1,], A. MARCINIAK[1], S. NANDI[1], G. KARRAS[1], M. HERVÉ[1], E. CONSTANT[1], E. PLÉSIAT[2], A. PALACIOS[2], F. MARTIN[2], F. LÉPINE[1]**

ABSTRACT. We present an interferometric HHG-2ω_0 scheme and compare it to the usual XUV-IR RABBIT method that is widely used in attosecond science. Both methods are able to reconstruct the properties of an attosecond pulse train and can be used to measure attosecond ionization time delays in atoms and molecules. While they have several similarities, they also have conceptual differences. Here, we present some particularities of the HHG-2ω_0 method and its advantages and drawbacks, which would help to define situations where it can provide information inaccessible by other technics.

Keywords: *Attosecond, Photoionization, RABBIT*

INTRODUCTION

With the advent of attosecond science (1 as= 10^{-18} s), it is now possible to have access to the natural timescale of electronic motion [1,2]. The extreme-ultraviolet (XUV) one-photon ionization of an atom or a molecule produces an electron in the continuum with a kinetic energy that depends on the interaction properties with the ionic core [3]. While the electron escapes, it experiences the interaction with its parent ion, and it can therefore be used as a probe of the ionic potential. Depending on these forces, the emitted electron can be attracted (*resp.* repelled) by the potential, which can be interpreted as an advance (*resp.* delay) on the ionization time. Such electron dynamics contain the details of the fundamental photoelectric process, thus unravelling the structure of the continuum of an atom or a molecule [4].

---

* *Presented at the First Annual Workshop for the COST Action Attosecond Chemistry (ATTOCHEM) CA18222, organized on-line, September 9-11, 2020.*

[1] *Univ Lyon, Univ Claude Bernard Lyon 1, CNRS, Institut Lumière Matière, F-69622, VILLEURBANNE, France.*

[2] *Departamento de Química, Modulo 13, Universidad Autónoma de Madrid, 28049 Madrid, Spain, EU.*

** *Corresponding author: vincent.loriot@univ-lyon1.fr*

Nowadays, it is experimentally possible to observe electron dynamics in time-resolved experiments, thanks to the development of High-order Harmonic Generation (HHG). HHG provides a table-top solution to produce attosecond pulses with a high degree of reproducibility and an intrinsically low temporal jitter between the XUV and the fundamental pulse. One way to probe attosecond dynamics is the RABBIT (Reconstruction of Attosecond Beating by Interference of Two-photon Transitions) method [5]. It employs an attosecond pulse train (APT) generated by HHG in gas, spatio-temporally overlapped with a perturbative dressing field. Both beams are produced with the same femtosecond laser source at the central frequency (ω_0). Measuring the photoelectrons resulting from the interaction between an atomic or molecular target with XUV pulses with attosecond accuracy allows measuring the photoionization time delay with both temporal and spectral resolution [6]. This powerful method has demonstrated its relevance in many physical systems [6-9]. The method is well suited for small atomic targets that can usually be considered as a single active electron system. However, for more complex targets, with more than one active electron and with extra degrees of freedom, this method can still work [8] but suffers from a rapid congestion of the experimental signal [10].

Recently, we proposed a variant of the RABBIT method that allows the experimental separation of the attosecond dynamics of a two active electron system [11]. The principle is to use a $2\omega_0$ dressing photon energy (instead of ω_0 for the RABBIT method) to avoid introducing new features (sidebands) in the XUV induced photoelectron kinetic energy spectrum (KES). Following this scheme, the photoelectron KES does not significantly vary with the XUV-$2\omega_0$ delay. Nevertheless, the attosecond information remains encoded in the angle of ejection of the electron in the laboratory frame. Hence, it becomes possible to recover the attosecond information by measuring the angularly resolved photoelectron KES as a function of the relative delay between the two pulses. This can be performed using a velocity map imaging (VMI) spectrometer [12] that is well suited for this purpose. The measurement of the time-resolved anisotropy parameter allows for the reconstruction of the electron dynamics.

This method can be used as an alternative approach to the RABBIT technique to both reconstruct the attosecond pulse train [13] and the photoionization time delays in molecules [11]. This scheme is not limited to the experimental arrangement presented here, it can also take place under different experimental configurations. For instance, an equivalent configuration can be obtained by generating both even and odd harmonics ($HHG_{even+odd}$) dressed by a perturbative pulse centered around ω_0. $HHG_{even+odd}$ can be performed in a gas target using a pulse composed by a

combination of ω_0 and $2\omega_0$ carrier fields locked in phase [14,15]. Also $HHG_{even+odd}$ can be generated in a non-centrosymmetric media such as HHG from plasma mirror [16]. Time resolved photoelectron measurements obtained by the interaction of an $HHG_{even+odd}$ dressed by an ω_0 photon is equivalent to the HHG-$2\omega_0$ presented here (*i.e.* $HHG_{odd\text{-}only}$-$2\omega_0$). In both cases, the dressing field couples the consecutive harmonics to each other.

In the present work, we first present the HHG-$2\omega_0$ method in details: its experimental implementation, the produced signal, its particularities, and specific analysis. Second, we show an example of extraction of the ionization phase differences between two electronic states from an experimental signal. Finally, the differences with the RABBIT method are discussed.

METHOD

HHG in gas targets generated by a linearly-polarized femtosecond laser pulse centered around the central frequency (ω_0) results in a spectral comb composed by odd harmonics of the fundamental laser frequency due to the centro-symmetric configuration [17]. Such harmonics are separated by twice the fundamental frequency ($2\omega_0$). HHG is a non-perturbative process, where the n^{th} order high harmonic yield does not follow the non-linear perturbation rule (yield$\propto I^n$), but the high harmonics can have similar intensities leading to an intensity plateau up to the cut-off energy given by $E_{max}=Ip+3.2Up$ [18] (with Ip the ionization potential of the generating atom and Up the ponderomotive energy). Using a fundamental central frequency (ω_0) in the near infra-red ($\hbar\omega_0$ up to ~1.5 eV), HHG leads to a frequency comb in the XUV range ($\hbar\omega_{XUV}$>10 eV). Since such harmonics are phase locked, the comb can correspond, in the temporal domain, to an attosecond pulse train (APT) [5,19].

The interaction of this APT with a single active electron system can lead to the ionization of the target because the XUV-photon energy is usually above the ionization potential of atoms and molecules. In the photoelectron KES, it results in peaks around the difference between the photon-energy and the ionization potential of the target ($\hbar\omega_{XUV}$-Ip_{target}). The measurement of the resulting angularly resolved photoelectron KES by itself (cf. Fig. 1(a,d)) does not allow to reconstruct the phase of the emitted photoelectron wave packet because it corresponds to a squared modulus of the amplitude probability. The traditional way to access phase information relies on the use of interferometric technics. To this aim, it is possible to use a weak dressing field that couples the ionization channels. Hence, quantum interferences can take place and they carry the information on the relative phases of the electron wave packets. The attosecond information can be retrieved by scanning the linear spectral phase of the dressing pulse, which corresponds, in the

time domain, to the delay between the APT and the dressing pulse. The RABBIT method proposes to use a single ω_0 photon to couple ionization channels between each other (Fig. 1(b,e)). This has the advantage to produce a signal on an *a priori* "background-free" photoelectron region and all the relevant information is gathered in the phase of the oscillation of the electron signal intensity. In contrast, the HHG-$2\omega_0$ method uses a single $2\omega_0$ photon field to couple the ionization channels (Fig. 1(c,f)). In this case, the oscillating signal is no longer measured on background-free conditions, and no significant changes can be observed in the angularly integrated photoelectron KES. However, the attosecond information remains present, and the oscillation appears as an asymmetric redistribution of the electron signal on each side of the laser polarization axis (vertical in Fig. 1). The electrons are preferentially redistributed either on the upper or lower side in the laboratory frame, involving odd β terms (β_{odd}) of the Legendre polynomial expansion to describe the photoelectron angular distribution [20]. This asymmetry oscillates with respect to the delay between the APT and the dressing pulse frequency ($2\omega_0$).

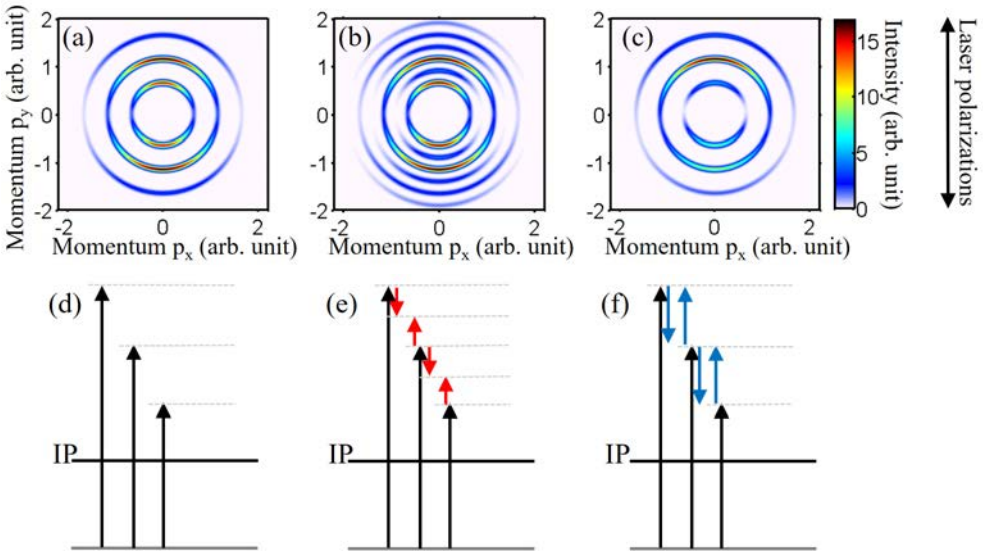

Fig. 1 *(a-c) Numerical simulation of the angularly resolved photoelectron distribution with a vertical polarization (along the p_y-axis) of the pulses where the APT pulse is (a) alone, (b) dressed by an ω_0 photon (RABBIT-scheme) and (c) dressed by a $2\omega_0$ photon (HHG-$2\omega_0$ configuration). (d-f) Energetic diagram corresponding respectively to (a-c). The harmonics (vertical black arrows) are ionizing an electronic state (gray solid line) to the continuum. The dressings photons (red arrows for RABBIT and blue arrows for HHG-$2\omega_0$) lead to the one-photon energy redistribution of the photoelectrons. Interferences occur at the energies indicated by horizontal dotted lines.*

In the present work, we consider the HHG-2ω_0 process under the lowest order of perturbation theory (i.e. weak dressing field). In this case, the resulting electron wave function depends on several ionization paths. The derivation of the dipole transition has been presented in Laurent *et al.* [14,15,21]. Different paths can lead to a given final photoelectron energy (see Fig.1(f)) as summarized in Table 1:

Table 1. Summary of the photo-absorption paths at the lowest order of perturbation theory, and the paths combinations that lead to a specific oscillating term in the interference.

Paths	$\hbar\omega_{XUV}$	*(i)*
	$\hbar\omega_{XUV} + \hbar\omega_{dress}$	*(ii)*
	$\hbar\omega_{XUV} - \hbar\omega_{dress}$	*(iii)*
Interferences	*(i) +(ii)* : β_{odd} ; Yield=constant ; Oscillation $2\omega_0$	(1)
	(i) +(iii) : β_{odd} ; Yield=constant ; Oscillation $2\omega_0$	(2)
	(ii)+(iii) : β_{even} ; Yield=vary ; Oscillation $4\omega_0$	(3)

*(i)*The direct absorption of an XUV photon ($\hbar\omega_{XUV}$), *(ii)* the absorption of an XUV photon and a dressing photon ($\hbar\omega_{dress}= 2\hbar\omega_0$), and *(iii)* the absorption of an XUV photon with a stimulated emission of a dressing photon. The interference (1) between the paths *(i)* and *(ii)* involves paths with a different number of photons. This results in an asymmetrical redistribution of the electron angular distribution with respect to the polarization axis (only β_{odd}) maintaining constant the yield (2π angular integration of the photoelectron distribution). The corresponding oscillation is expected at the dressing field frequency ($2\omega_0$). A similar scheme appears in the interference (2), between the paths *(i)* and *(iii)* producing electrons at the same final kinetic energy.

The interference (3) can take place between the paths (*ii*) and (*iii*). This interference corresponds to the RABBIT-like scheme, as shown in Fig.1 (e) where the central harmonic does not play any role. This interference is significantly different from the interferences (1) and (2) because, in this case, both paths involve the same number of photons leading to an interference that significantly changes the photoelectron KES. Since the transition parity is preserved, a symmetric redistribution of the electrons on each side of the polarization axis (β_{even}) is expected. This pattern may oscillate at twice the dressing field photon energy, hence at $4\omega_0$. The interference (3) can easily be distinguished from the interferences (1) and (2) by measuring the oscillation frequency and the electron ejection anisotropy. Moreover, the interference (3) is expected to appear at higher dressing field intensity because more than one-dressing photon is involved in the process.

The interferences (1) and (2) can be treated separately, their resulting intensities are summed up [14]. The asymmetric oscillation $\Delta S_n(t)$ of the angular distribution that appears on the top of the XUV-only harmonic peaks (of the order *n*) can be written as:

$$\begin{aligned}\Delta S_n(t) = \quad & A_n A_{n-2} \cos(2\omega_0 t + \varphi_{n-2} - \varphi_n) \\ & - A_{n+2} A_n \cos(2\omega_0 t + \varphi_n - \varphi_{n+2}),\end{aligned} \tag{4}$$

with *t* being the delay between the APT and the dressing pulse (*t*>0 corresponds to a dressing pulse that arrives later). A_n and φ_n are respectively the amplitude and phase of the one-photon ionization following the absorption of the n^{th} order harmonic. Similarly, $A_{n\pm2}$ and $\varphi_{n\pm2}$ denote the corresponding amplitude and phase of the two-photon ionization following the absorption of a photon at the harmonic order *n±2* accompanied with the one-photon emission or absorption of the dressing field. The amplitudes *A* depend on the photo-absorption cross-section and the HHG and dressing field intensity. The phases φ contain the dipole transition phase, the harmonics phase and the Coulomb interaction phase. The two contributions are oscillating at $2\omega_0$ frequency, so their sum also oscillates at the $2\omega_0$ frequency. The experimental signal $S_n(t)$ at the harmonic location *n* can hence be re-written as a simple oscillation as follows:

$$S_n(t) = B_n \cos(2\omega_0 t + \phi_n), \tag{5}$$

where B_n and ϕ_n are respectively the global oscillation amplitude and phase on the top of the harmonic *n*. Only B_n and ϕ_n terms are experimentally measurable by recording the time-resolved photoelectron KES on one side of the laser polarization axis. The measurable parameters (B_n and ϕ_n) are both depending on 6 parameters (A_n, A_{n-2}, A_{n+2}, φ_n, φ_{n+2}, φ_{n-2}).

As a comparison, in the usual RABBIT method, an oscillation of the yield is observed in the sidebands with respect to the delay between the pulses. The sideband oscillation phase can be established from the phases φ_{n+1} and φ_{n-1}, and the sideband oscillation amplitude from the amplitudes A_{n+1} and A_{n-1}. At the lowest order of perturbation theory, the dressing field does not ionize, but redistributes the photoelectron intensity over different electron kinetic energies. Hence the RABBIT photoelectron yield on the harmonics peaks (bands) are also oscillating maintaining constant the total ionization yield. The oscillation of such bands depends on the interferences with the surrounding sidebands. Therefore, this band oscillation is comparable with the one of HHG-$2\omega_0$ method, because its expression is similar to the

one presented in Eq. 4 with both terms negative (not only the second one). In the RABBIT method, despite that all the relevant information can be extracted from the sideband oscillation amplitude and phase, the analysis of the bands can also be used to refine the reconstruction due to the redundancy of the information [22]. Both bands and sidebands indeed encode the same (A, φ) parameters in a different way.

The correspondence between (A, φ) and (B, ϕ) is not straightforward. The measured (B, ϕ) can dramatically change by slightly changing (A, φ). The (A, φ) terms can both be set experimentally using XUV optics such as metallic filters [23] that can modify the harmonic distribution and/or its spectral phase. In the following, we show the typical changes in (B, ϕ) due to amplitude (Fig. 2(b,e)) and phase (Fig. 2(c,f)) shaping, from a reference condition (Fig. 2(a,d)).

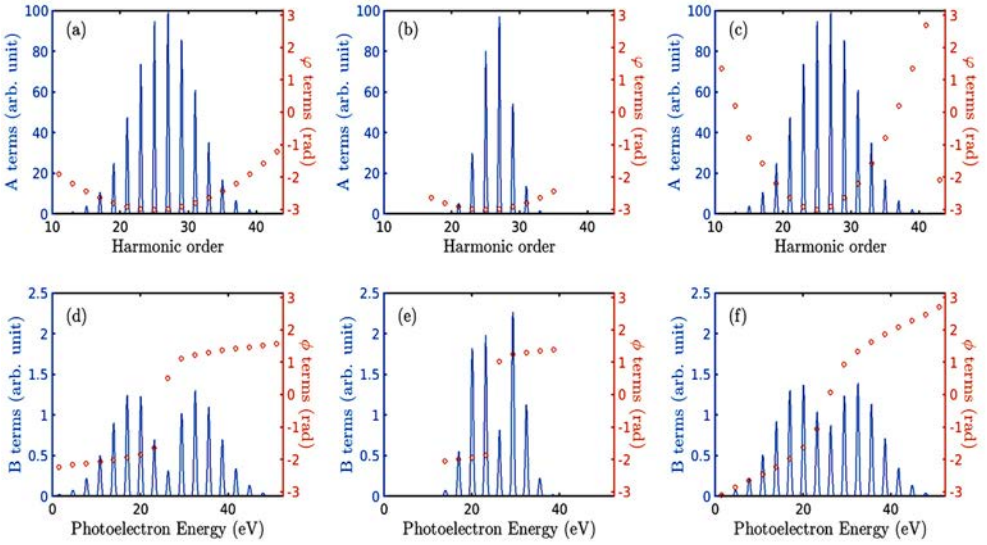

Fig. 2. *Numerical simulation of Eq. 4 corresponding to the HHG-2ω_0 method. (a-c) are the (A, φ) terms in solid blue line and orange circles respectively. (b) corresponds to an amplitude narrowing of (a), (c) four times stronger parabolic spectral phase compared to (a). (d-f) The corresponding amplitude B (blue) and phase φ (orange) of the 2ω_0 oscillation using the respective spectra shown in (a-c). In the simulation, the ionization potential has been chosen to be 15.6 eV (close to the Ip of N_2 and Ar), and $\hbar\omega_0$=1.55 eV.*

The reference (A, φ) condition shown in Fig. 2(a) represents a comb of harmonics with a Gaussian envelope and a small quadratic spectral phase (chirp) of 2000 as². Its corresponding oscillation, (B, ϕ) terms, are shown in Figure 2(d). The chirp appears as a linear distribution of the ϕ phase terms due to the consecutive phases

differences in Eq. (4). On the top of this tendency, a phase–jump (about π) appears close to the maximum of the Gaussian envelope. It corresponds to a sign change in the equation (4) where the term $(A_{n-2}\text{-}A_{n+2})$ becomes positive or negative (*i.e.* $-1=e^{i\pi}$). This implies a change in the most intense term in Eq. 4. In a first approximation, the *B* term distribution follows the product between the Gaussian envelope and its derivative, showing the highest oscillation where the slope of the envelope is pronounced.

The narrowing of the *A* distribution by a factor of 4 (maintaining φ shape constant) leads to significant changes in both (B, ϕ) terms (see Figure 2 (b) and (e)). The linear slope in φ_n is still apparent, and the phase–jump is more pronounced due to a sharper difference between the $(A_{n-2}\text{-}A_{n+2})$ coefficients. The *B* amplitudes distribution is narrowed and more pronounced compared to the reference due to a significant change in the (A_{n-2}/A_{n+2}) ratio. A moderate narrowing of the *A* terms can lead to a very different set of (B, ϕ) terms.

An increase by a factor 4 of the quadratic chirp (maintaining the A terms distribution) also leads to significant changes in both (B, ϕ) terms (see Figure 2 (c) and (f)). The resulting phases φ are linearly increasing with a stronger slope with a smooth phase-jump. On the other hand, the oscillation amplitudes *B* are enhanced compared to the reference because the terms in equation 4 do not efficiently cancel each other.

In general, the use of an XUV filter affects both the amplitude and the phase of the harmonics that directly modify the (A, φ) set. Such changes can dramatically affect the (B, ϕ) distributions due to the coupling between the parameters. Let us notice that the flat phase case over an *A* terms plateau produces the lowest oscillation amplitude *B* increasing required performances of the experiment. This flat phase case is usually sought because it corresponds to the shortest attosecond bursts (when atomic/molecular effects are weak).

In order to characterize a light-matter interaction, it is usually necessary to reconstruct the amplitude and the phase terms (A, φ) from an experimental measurement (B, ϕ). This task is not straightforward because of the high dimensionality of the problem and the correlation between the parameters. An experimental example is presented in the following.

EXPERIMENT

In a recent work, we used the HHG-$2\omega_0$ strategy to extract the relative ionization time delay between two electronic states of the N_2 molecule [11]. The two uppermost levels, the *X*-state ($^2\Sigma_g^+$, Ip_X=15.6 eV) and the *A*-state ($^2\Pi_u$, Ip_A=16.98 eV) in N_2^+ ions are separated from each other by 1.4-1.7 eV in the photoelectron KES,

depending on the vibration level of the *A*-state. Following a standard RABBIT protocol using a standard Ti:Sa femtosecond-Laser as a seed ($\hbar\omega_0$=~1.5 eV), the bands of an electronic state can overlap with the sidebands of the other electronic state [24]. In that case, an HHG-2ω_0 protocol is well suited to separate the dynamics of the electronic states of this molecule.

In the *X*-state of N_2^+, a shape resonance appears at photon energy around 30 eV [25]. The shape resonance has two consequences, first the absorption cross-section experiences a maximum and second the phase of the escaping electron is significantly affected. A rapid change in the phase (φ), as a function of the photon energy (E), can be interpreted as a delay in the photoionization time, following the Wigner theory [26] $\tau_w=\hbar\partial\varphi/\partial E$. Since the *X* and *A* states are measured in similar experimental conditions, all the sources that affect the observations (phase of the harmonics, continuum-continuum phase, ...) can be considered as identical. The energy difference between the two states is small, and the *A* state has no resonance in this spectral region ($\tau_w(A)\approx0$). Therefore, it is possible to use the *A*-state as a reference to measure the dynamics induced by the shape resonance in the *X*-state.

The experimental measurement is shown in Fig. 3. The measurement shown in Fig.3(a) represents the photoelectron distribution angularly integrated over the upper part of the VMI detector (over the range [-π/2 : π/2] with respect to the laser polarization axis) as a function of the time delay between the XUV and the dressing pulse. Since the attosecond oscillations represent only a few percent of the overall signal, the photoelectrons generated by the XUV-pulse measured alone have been subtracted to highlight the oscillating part of the signal in Fig. 3(a).

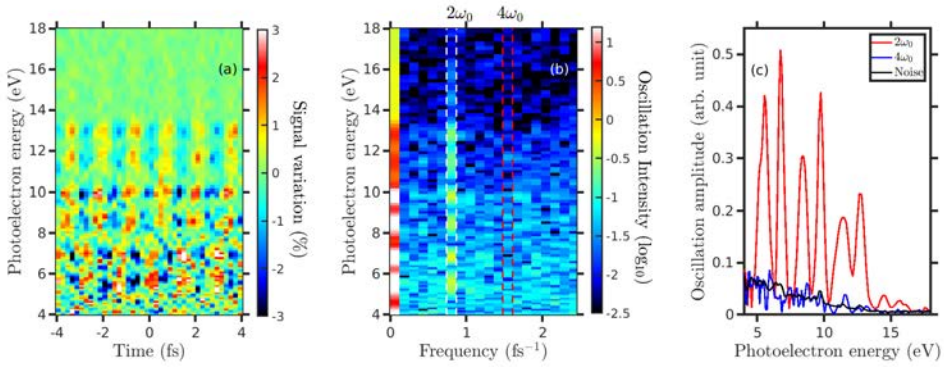

Fig. 3. *(a) HHG-2ω_0 measurement in N_2 (adapted from [11]) and (b) its corresponding Fourier transformation resolved in kinetic energy. (c) Amplitude of oscillation at 2ω_0 (red) and 4ω_0 (blue) compared to the mean oscillation amplitudes (black) of the Fourier transformation at other frequencies.*

The Fig. 3 (b,c) shows the amplitudes of the oscillations as a function of the photoelectron energy. The oscillation amplitudes are extracted by performing a Fourier transformation of the temporal signal for the measured kinetic energies considered individually. Note that the amplitude is in log-scale which illustrates the difference in two orders of magnitude between the XUV-only photoelectron distribution (frequency=0 fs^{-1}) and the HHG-$2\omega_0$ oscillation (frequency=0.75 fs^{-1}, *i.e.* period of 1.33 fs). Fig. 3(c) shows the oscillation amplitude in a linear scale and compares them with the estimated noise level that is taken as the mean oscillation amplitude of the other frequencies (all frequencies except 0, 0.75 and 1.5 fs^{-1}). This figure shows a SNR of about 10 between the amplitude of oscillations at $2\omega_0$ compared to the estimated noise level. It can be noticed that no oscillation is observed at the $4\omega_0$-frequency (frequency=1.5 fs^{-1}, *i.e.* period of 666 as). This indicates that the dressing field is weak enough and does not produce significant RABBIT-like oscillations in the observable (interference path (3)).

In order to extract the ionization phases of the *X* and the *A* states of N_2, it is necessary to reconstruct the (A, φ) terms from both (B, ϕ) terms extracted from the measurement shown in Fig. 3. An analytical reconstruction solution of the φ terms has been proposed by Laurent *et al.* [15] (iPROOF) from the experimental (B, ϕ) assuming that the *A* terms are measured separately. In principle, the *A* distribution can be associated to the photoelectron KES measured when the XUV pulse is alone. In our case, we do not strictly follow this principle because the focal size of the harmonics depends on their wavelength leading to a different effective overlap with the dressing field. In our case, the *A* terms are considered as free parameters, but the reconstructed effective HHG spectrum may gradually follow the directly measured HHG distribution. The reconstruction is given by an optimization algorithm that directly uses the equation 4. The determination of the initial guess is critical due to the presence of several local optimums in the optimization landscape.

Figure 4 shows the result of the extraction of the relative ionization phase between the *X* and *A*-states in N_2. The reconstruction of (A, φ) is performed for the two states considered separately. The experimental *B* term (Fig. 4(a)) is defined by integrating the oscillation over the peak width. The corresponding experimental phase is the center of mass of the phase over the width of the peak weighted by the oscillation amplitude terms. The reconstruction of the amplitudes *A* is not exactly the same for the two states due to slightly different photo-absorption cross-sections. The φ terms shown in Fig. 4(e) present a slightly different behavior. Fig. 4(c) shows the first derivative of the phases for the two states considered separately. This term is defined as the difference between two consecutive reconstructed φ phases and is centered between the two considered harmonics orders. In this illustration, the

shape of the *A*-state is mainly due to the harmonics and the continuum-continuum phases since the molecular phase is assumed to be negligible in this energy region. The difference between the measurements are mainly due to differences in the derivatives of the phases of the dipole matrix elements describing the transitions to the *X* and *A* states. This provides the difference in ionization time delay between the two states. Ionization delays up to 50 attoseconds have been measured experimentally on the peak of the shape resonance around 30 eV (around the harmonic order 20), and positive delays are also observed at lower photon energies [11].

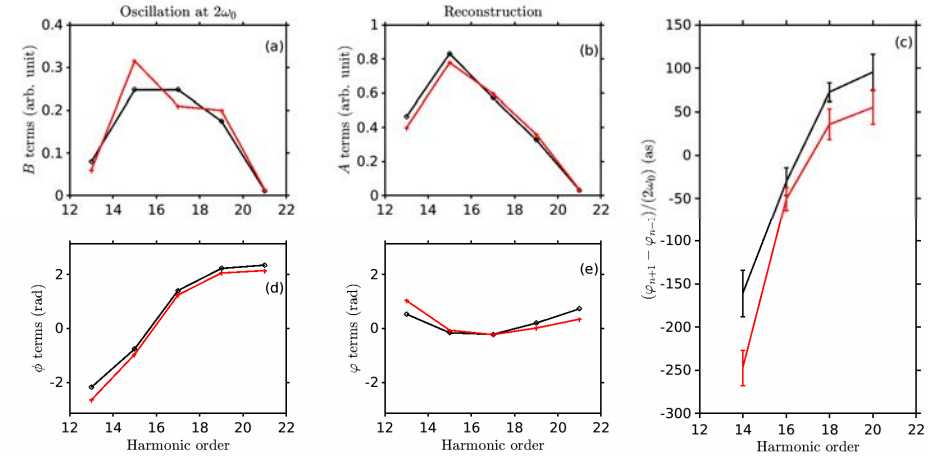

Fig. 4. *Reconstruction of the ionization phase differences between the X and A-states of N_2^+ represented in black and red respectively. Measured amplitude B (a) and phase ϕ (d) of oscillation at $2\omega_0$. Reconstructed amplitude A (b) and phase φ (e) terms and (c) the corresponding phase derivative of the two states, considered separately, in attoseconds.*

CONCLUSION

The HHG-2ω_0 scheme is an alternative solution to the RABBIT method that provides the same attosecond information on the dynamics of a quantum system. However, the HHG-2ω_0 and RABBIT methods have significant conceptual differences. The HHG-2ω_0 method does not significantly change the photoelectron KES but relies on electron momentum β_{odd} asymmetry, while the RABBIT method duplicates the number of contributions that oscillate with the sidebands appearance described by β_{even} angular terms. In the HHG-2ω_0 method, both the spectral amplitude and phase of the initial pulse has an influence on both the amplitude and the phase of the

oscillations. In RABBIT, only the system's phases play a role on the phases of the sideband oscillations. The HHG-$2\omega_0$ scheme provides a better contrast when using a harmonic comb that has a rapidly varying envelope and a non-flat phase, while RABBIT sidebands measurements exhibit a higher contrast. Let's notice that the analysis of the RABBIT oscillation measured over the harmonics peaks is conceptually close to the HHG-$2\omega_0$ method. The reconstruction of the HHG-$2\omega_0$ method involves both the amplitude and phase of the experimental oscillation. In both methods, the attosecond oscillations appear at twice the dressing field $2\omega_0$. Both methods allow us to reconstruct the temporal profile of an attosecond pulse train [13, 15] and measure the ionization time delay in atoms and molecules [11, 24, 27].

The present HHG-$2\omega_0$ method is however unique when photoionization proceeds through several open channels, which leads to spectral congestion in the usual RABBIT measurements due to many overlapping contributions. This is already the case for small molecules such as nitrogen [11] and atoms with a strong spin-orbit coupling such as Xenon, so that one can expect that the HHG-$2\omega_0$ method would be even more useful in complex molecules where the number of ionization channels is much larger. Also, it is of interest when both even and odd harmonics are generated and more generally, in all the configurations where only one attosecond pulse is present per optical cycle of the dressing field [14, 16, 28].

Nowadays, many RABBIT-like interferometric scheme appear to access the attosecond information under various experimental conditions. For example, using the free-electron-laser radiation, the harmonics are separated by $3\omega_0$ and the system can be dressed by one and two ω_0 photons [29]. The development of different interferometric configurations can extend the "toolbox" of attosecond science to get suitable experimental arrangements for the study of attosecond dynamics in a large variety of quantum systems.

ACKNOWLEDGMENTS

We acknowledge the support of CNRS, ANR-16-CE30-0012 "Circé", ANR-15-CE30-0001 "CIMBAAD" and the Fédération de recherche André Marie Ampère. EP, AP and FM are supported by the MINECO grant FIS2016-77889-R. FM acknowledges support from the "Severo Ochoa" Programme for Centres of Excellence in R&D (MINECO, Grant SEV-2016-0686) and the "Maria de Maeztu" Programme for Units of Excellence in R&D (MDM-2014-0377).

REFERENCES

1. M. J. J. Vrakking, F. Lépine, "Attosecond Molecular Dynamics", The Royal Society of Chemistry, 2019.
2. D. Baykusheva, H. J. Wörner, "Attosecond Molecular Spectroscopy and Dynamics", Elsevier, 2020, chapter 3.
3. U. Becker, D. A. Shirley, "VUV and Soft X-Ray Photoionization", Plenium Press, New York, 1996.
4. R. Pazourek, S. Nagele, J. Burgdörfer, *Rev. Mod. Phys.*, 87, 765 (2015).
5. P. M. Paul, *et al., Science,* 292, 1689 (2001).
6. M. Isinger, *et al., Science,* 358, 893 (2017).
7. V. Gruson, *et al., Science*, 354, 734 (2016).
8. M. Huppert, *et al., Phys. Rev. Lett.*, 117, 093001 (2016).
9. M. Kotur, *et al., Nat. Commun.*, 7, 10556 (2016).
10. I. Jordan, *et al., J. Opt.*, 20, 024013 (2018).
11. V. Loriot, *et al., J. Phys.: Photonics,* 2, 024003 (2020).
12. T. J. B. Eppink, D. H. Parker, *Rev. Sci. Instrum.*, 68, 3477 (1997).
13. V. Loriot, *et al., J. Opt.*, 19, 114003 (2017).
14. G. Laurent, *et al.*, *Phys. Rev. Lett.*, 109, 083001 (2012).
15. G. Laurent, *et al.*, *Opt. Express*, 21, 16914 (2013).
16. C. Thaury, F. Quéré, *J. Phys. B*, 43, 213001 (2010).
17. A. L'Huillier, Ph. Balcou, *Phys. Rev. Lett.*, 70, 774 (1993).
18. P. B. Corkum, *Phys. Rev. Lett.*, 71, 1994 (1993).
19. R. Lopez-Martens, *et al., Phys. Rev. Lett.*, 94, 033001 (2005).
20. R. N. Zare, "Angular momentum", Wiley & Sons, Inc., New York, 1988
21. G. Laurent, *et al.*, *J. Phys. Conf. Ser.*, 488, 012008 (2014).
22. Y. Mairesse, F. Quéré, *Phys. Rev. A*, 71, 011401(R) (2005).
23. B.L. Henke, E.M. Gullikson, J.C. Davis, *At. Data Nucl. Data Tables*, 54, 181-342 (1993).
24. S. Haessler, *et al., Phys. Rev. A*, 80, 011404(R) (2009).
25. R. R. Lucchese, K. Takatsuka, V. McKoy, *Phys. Rep.*, 131, 147 (1986).
26. E. P. Wigner, *Phys. Rev.*, 98, 145 (1955).
27. S. Nandi, *et al.,* Sci. Adv., 6, eaba7762 (2020).
28. J. Mauritsson, et al., Phys. Rev. Lett., 100, 073003 (2008).
29. P. K. Maroju, *et al., Nature*, 578, 386 (2020).